Achilles and GENIE Model Comparisons Between Quasi-Elastic Proton Exclusive Events in DUNE PRISM ND-LAr

Andrew Garcia and Minerba Betancourt
Fermi National Accelerator Laboratory, Batavia, IL 60510
December 4, 2024

1 Abstract

In this study, we analyze simulated CCQE proton exclusive events in DUNE's ND-LAr using Achilles and GENIE Monte Carlo event generators. We generate events using muon neutrino exclusive flux files of DUNE's on-axis and 20m off-axis PRISM positions and compare various kinematics of proton exclusive events between the event generators. Events are further analyzed in categories according to the number of final-state protons. This study was motivated by QE's dominance in statistics for off-axis events over other channels in which off-axis events are very useful for characterizing DUNE's flux. Furthermore, our motivation for comparing results between generators is driven by off-axis QE neutrino spectra peaking below 1 GeV. In this region, many low-energy proton events are produced in which models have been shown to have disagreements.[1]

2 Introduction and Background

DUNE is multipurpose international neutrino detection experiment currently under construction at the Long-Baseline Neutrino Facility (LBNF) in Fermilab, Illinois, and Sanford Underground Research facility, South Dakota. The primary aspect of the project consists of sending a flux of neutrinos produced at Fermilab 1300km through the surface of earth in which near detectors (NDs) and a far detector (FD), positioned at Fermilab and Sanford respectively, will measure initial and oscillated flux spectra. The neutrino beam, powered the PIP-II project, will be the most intense experimentally produced flux of neutrinos in history, capable of producing significantly more events compared to previous experiments.[2]

The ND consists of three detectors, one of which is a liquid argon time projection chamber (LArTPC) and is the focus of our study (See FIG. 1 for

[1] journals.aps.org/prl/pdf/10.1103/PhysRevLett.133.041801
[2] https://www.dunescience.org

diagram). Events in the ND-LAr are comparable to the FD due to them both being LArTPCs and thus, analysis directed toward the ND-LAr is applicable to the FD. In the ND-LAr, neutrinos interact with argon nuclei producing leptons and hadrons which create ionization tracks indirectly detectable by PMTs and wire planes. This detection method allows for a full 3d reconstruction of the ionize tracks and thus the kinematics of final-state particles in the interaction.

The ND-Lar is a special LarTPC such that it can be moved transverse to the neutrino beam to detect various off-axis events. This allows for more statistics of similar-type events in the FD and greatly helps to classify the flux according to the PRISM concept.[3]

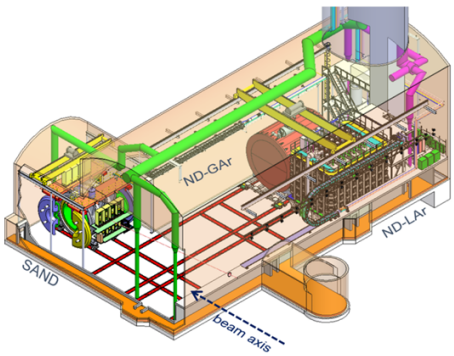

Figure 1: Diagram of the DUNE ND

2.1 Interaction Channels

There are many channels in which a neutrino can interact with an argon nuclei. The channels are divided into two main categories: charged current (CC), in which the interaction is mediated by a W boson, and neutral current (NC), mediated by the Z boson. The primary interaction channels that contribute most prominently in total ND events are: quasi-elastic scattering (QE), deep-inelastic scattering (DIS), resonant pion production (RES), meson exchange current (MEC), and NC as a general category. In this study, our main focus is QE events motivated by its dominance in off-axis events as seen from simulated data.[4]

Due to each channel being a different physical process, events by channel type differ in final-state particles and kinematic distributions. In theory, the neutrino's energy and flavor are determined by specifying all final-state particles and their kinematics, but in practice this is not accomplished. Some final-state

[3]https://indico.cern.ch/event/857610 /contributions/3654728/attachments/1957122 /3251362/DUNE-ND-Overview-LBNC-Dec2019.pdf

[4]Data from GENIE AR23_20i hA2018 using DUNE fluxes obtained from: pnfs/dune/persistent/physicsgroups/dunelbl/abooth/PRISM/Production/Simulation /ND_CAFMaker/v7/CAF

particles are not easily detectable and final state nuclei energies are unknown. Thus, is crucial to understand and identify interaction channels to infer the missing information needed to reconstruct the neutrino energy.

2.2 Event Generators

As stated in the above discussion, reconstruction of the neutrino energy from final-state observables is not straight-forward. Given a set of all final-state particles and their kinematics we are still missing energy content contained in nuclear effects that is needed for the full reconstruction. Thus, proper modeling of these interactions to understand nuclear effects and distinguish channels apart is key.

A common approach is the use of Monte Carlo event generators which sample an input flux of incident particles and generate scattering events based on their models. However, due to the complexity of interactions with nuclei, there are no single agreed open modeling choices. Because of this, models tend to differ and produce different results for specific cases. the main modeling choices happen in the primary interaction, how the nuclear medium of nuclei are treated, and how final state interactions (FSIs) are handled as hadrons propagate through the nuclear medium before escaping.

In this study we look at the event generators called GENIE and Achilles. In the below table we outline some of the model differences we found between them.

Generator	QE Model	Nuclear Model	Form Factors
Achilles	Spectral function approach	LocalFGM	Vector: Kelly Axial: z-expansion https://arxiv.org/abs/0708.1946
GENIE (AR23_20i)	Nieves, RPA	LocalFGM	Vector: BBBA parameterization Axial: z-expansion [0708.1946] Vector and Axial Nucleon Form Factors:A Duality Constrained Parameterization

FSI Model	Pauli-Blocking	Cascade
Achilles	Yes	Yes (INLC like)
hA2018	No https://arxiv.org/pdf/2103.07535	No (uses fits from data) https://arxiv.org/pdf/2103.07535
hN2018	No https://arxiv.org/pdf/2103.07535	Yes https://arxiv.org/pdf/2103.07535

Figure 2: Main comparisons we found between Achilles and GENIE models.

Without going into much detail, we found that Achilles and GENIE use different QE models, vector form factors, and FSI models. [5] Since GENIE has

[5] See the following for more information on GENIE FSI models and nuclear models in general: https://arxiv.org/pdf/2103.07535. Missing sources are due to information gained through direct discussion with developers.

multiple FSI models, our analysis consists of producing data sets with each FSI.

3 Methods

Events in this study are self-generated and analyzed at truth level. The input flux used is muon exclusive with 100,000 QE exclusive events generated for all cases mentioned below.[6] We filter events by the number of final-state protons they possessed, specifically looking at events with a single proton ($n_p = 1$), events with two protons ($n_p = 2$), and events with more than two protons ($n_p > 2$). We create tables to distinguish event numbers for the different models and create histograms to analyze various kinematics. As parameters, we vary PRISM ND axis position, and final-state interactions on/off. We also toggle on/off a momentum cut of 0.3 GeV on the analyzed protons, representing the current liquid argon detector sensitivity. This cut is implemented after checking if a final-state particle is a proton: if a final-state particle is a proton, its momentum is checked and then the further analysis is done.

4 Results and Analysis

In this section we discuss and analyze the results of our generated events. We split these results into four major subsections. In the first subsection, we briefly discuss the neutrino flux's dependence on PRISM ND position followed by the our results on predicted muon kinematics. Specifically, we look at muon energy, z-momemtum, and scattering angle. In the second subsection, we discuss the differences between models for single proton events with FSIs off. In the third subsection, we compare proton kinematics with FSIs on and analyze results by the number of final state protons. For the proton analysis, we look at leading/subleading proton energies and the angle between the muon and leading proton. Finally, in the fourth subsection, we brief discuss similarities we found between kinematics produced using DUNE's 20m off-axis flux and MicroBooNE flux.

4.1 Axis position Dependence on Neutrino Spectra and Muon Kinematics

We begin by mentioning the neutrino flux's dependence on axis-position. Below in FIG. 3, we can see that the neutrino flux distribution becomes more mono-energetic and shifted to lower energies as position increases. This difference leads to more spread out higher energy incident neutrinos for on-axis events and more focused lower energies for large off-axis events.

[6] Input fluxes obtained from: /pnfs/dune/persistent/physicsgroups/dunebeam/ikotler /DUNE_PRISM.

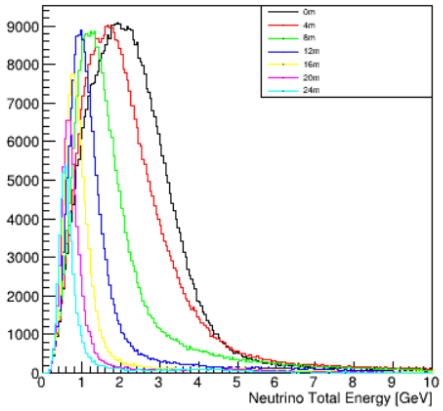

Figure 3: QE muon neutrino flux spectra at varying axis positions.

To discuss our results, we compare all kinematic distributions using on-axis and 20m off-axis fluxes as representative samples for small and large off-axis positions. This choice is due to differences caused by axis-position varying smoothly, so we pick two extremes.

We now discuss the muon kinematics. Below in FIG. 4 are distributions for muon energy, z-momentum, and scattering angle. We summarize the results by showing events with any number of protons as we saw that the distribution shapes remained mostly independent of proton case.

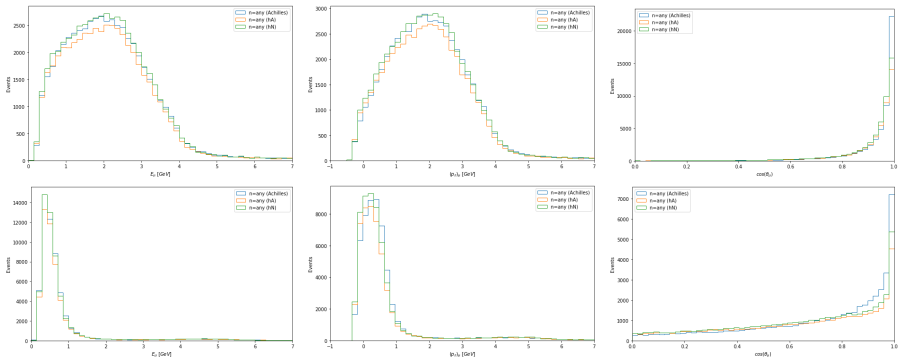

Figure 4: Muon kinematics in events with any number of protons. The top plots are on-axis and the bottom 20m off-axis.

In FIG. 4, we can see that all three models agree across kinematics and axis positions besides a slight difference in 20m off-axis scattering angles. We observe that Achilles diverges from the GENIE models, picking up more events at small scattering angles. To pick out the cause of this difference, we remove

final state interactions and add in the momentum cut on the protons as plotted below in FIG. 5.

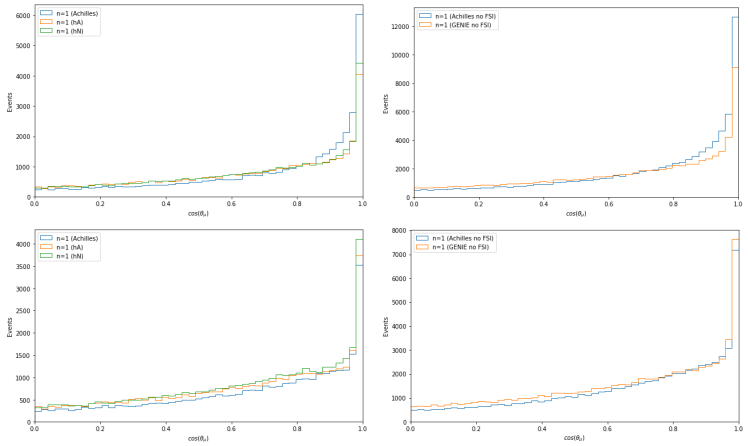

Figure 5: 20m off-axis muon scattering angle. Top left: with FSI, top right: without FSI, bottom left: with FSI and with cut, bottom right: without FSI and with cut.

In FIG.5 we see that taking away FSI effects does not remove Achilles' additional low-scattering events over GENIE. However, adding in the momentum cut on the protons does remove this feature. This indicates to us that this difference is caused by a correlation between low-momentum protons and small scattering angle muons which is not present in GENIE.

4.2 Proton Kinematics without FSI

We now look at our obtained proton kinematics from Achilles and GENIE without FSI. We begin by observing the differences in proton kinetic energy for the different cases. In FIG. 6, we plot our obtained spectrum below for both on-axis and 20m off-axis positions.

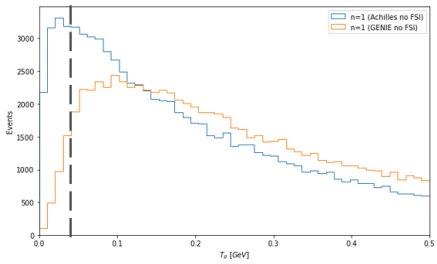

Event Type	$n_p = 1$
Achilles	86293
GENIE	95823

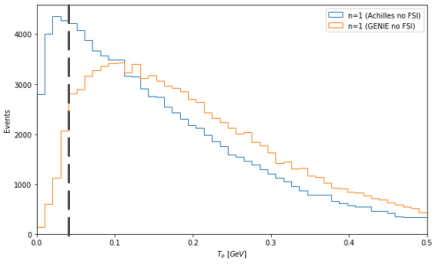

Event Type	$n_p = 1$
Achilles	82007
GENIE	94414

Figure 6: Proton kinetic energy distributions with on-axis on the left and 20m off-axis on the right. Tables are event numbers with the momentum cut added.

It is worth noting that since the primary QE interaction produces a single proton and turning off the FSI removes the cascade effect, we only have events with single final state protons. Thus, both generators produce exactly 100,000 events before the cut. However, when adding the cut, we see differences in the total events displayed in tables in FIG. 6. We observe that the cut removes significant more events for Achilles, indicating a larger production of low momentum protons in Achilles. This indicates a possible source for the 20m muon scattering angle differences we saw above.

We see further differences in the FIG. 6 histograms with Achilles' protons having a low kinetic energy peak below 0.05 GeV while GENIE possesses a much shallower peak at approximately 0.10 GeV. Observing the tails of the distributions shows us that GENIE produces more high energy events than Achilles as well. Thus, we see that Achilles favors lower energy protons in this specific case.

Since these events only have single protons, adding the momentum cut just corresponds to cutting all events below a certain kinetic energy shown by the dashed line. We can see that the cut does not change the distributions' agreement by very much. Comparing between 0m and 20m axis positions, we see a shift in events between low and high energies. When moving to high off-axis positions, high-energy events are relocated to low-energy events. However, we see this shifting of events is in such a way that does not displace peak locations or comparisons between generators.

We now look at our results for the angle between the muon and proton displayed below in FIG. 7.

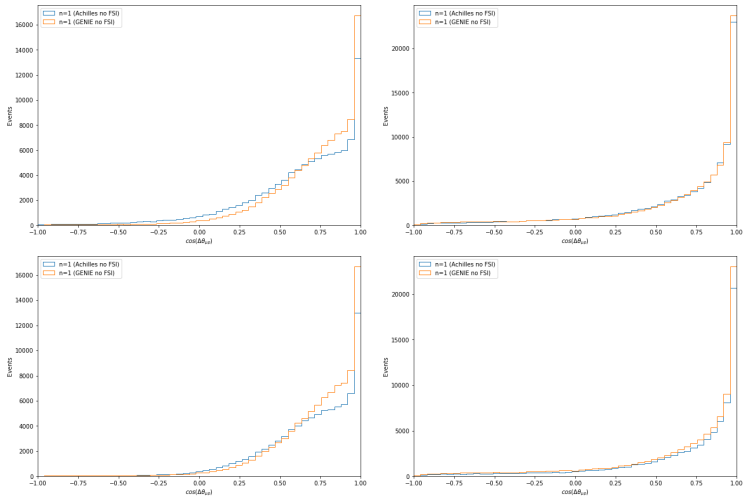

Figure 7: Angle between muon and proton distributions. Top plots are without the momentum cut and bottom plots are with. Left plots are on-axis and right plots are 20m off-axis.

Looking at on-axis events in FIG. 8, we see disagreement in which Achilles produces more large-scattering angle events while GENIE produces more events on the lower side. Adding in the momentum cut removes Achilles large angle events, but the small angle differences remain present. We see much better agreement in the 20m off-axis position indicating a neutrino energy dependence on these distributions.

The result of this analysis is that Achilles and GENIE differ before adding in FSI effects, indicating QE or form factor model dependencies causing Achilles to favor low energy protons. We also see differences in the angle between the muon and proton that vanish when the flux is more mono-energetic with lower energies.

4.3 Proton Kinematics with FSI

We now observe the effects of adding the differing FSI models to the proton kinematics. Since FSIs allow for the production of many protons in the final-state, we look at cases with single, two and greater than two protons to analyze differences more deeply. We first summarize the differences in event number for each case in TAB. 1 below.

Event Type	$n_p = 1$	$n_p = 2$	$n_p > 2$	Total
Achilles	45791	9003	1781	56575
hA	46001	4147	1075	51223
hN	46555	6989	2336	55880

Event Type	$n_p = 1$	$n_p = 2$	$n_p > 2$	Total
Achilles	46174	9104	1599	56877
hA	47130	4318	1113	52561
hN	47788	7610	2686	58084

Table 1: Left: on-axis, right: 20m off-axis.

In TAB. 1 we observe that all models have a similar number of $n_p = 1$ events. For $n_p = 2$ events Achilles leads followed by hN, and for $n_p > 2$, hN leads followed by Achilles. hA produces substantially less multi-proton events most likely due to its cascade model. These results hold for 20m off-axis as well. We now add in the momentum cut on protons and display results below in TAB. **??**.

Event Type	$n_p = 1$	$n_p = 2$	$n_p > 2$	Total
Achilles	41015	5910	623	47548
hA	46342	2380	460	49182
hN	48393	4364	407	53164

Event Type	$n_p = 1$	$n_p = 2$	$n_p > 2$	Total
Achilles	40198	4704	417	45319
hA	47344	2180	338	49862
hN	50219	4137	333	54689

Table 2: Left: on-axis, right: 20m off-axis.

In TAB. 2 we see that Achilles loses events from all categories when the cut is added. This indicates to us that the energy content is more spread out between the protons as if most of the energy was contained in the leading, we would see a shifting of events from multi-proton to $n_p = 1$. For both GENIE models, we see this is the case: hA and hN both lose events from multi-proton cases and gain events in $n_p = 1$. Thus, in multi-proton events, GENIE's leading proton appears to contain most of the energy out of the total proton energy in contrast to Achilles.

We now look at the differences in the proton kinematics with FSIs on. Below in FIG. 8 we plot the leading proton's kinetic energy for on-axis and the different proton event cases.

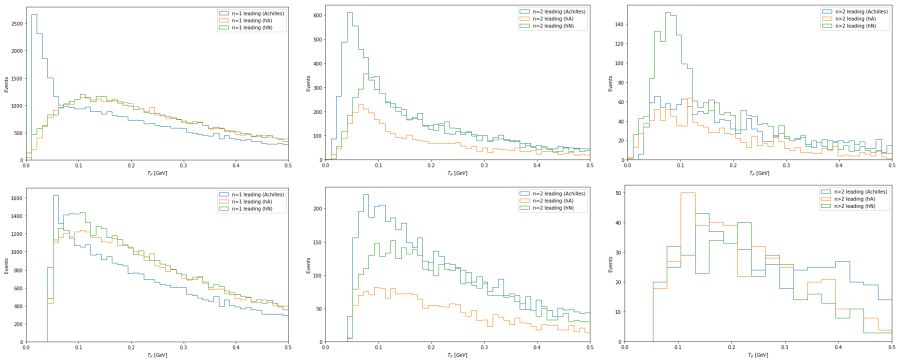

Figure 8: On-axis kinetic energy of leading proton. Top plots are without the cut and the bottom with. The left most plots are $n_p = 1$, middle plots $n_p = 2$, and right plots $n_p > 2$.

Observing the $n_p = 1$ case, we see that the differences between Achilles and the GENIE models are similar to FIG. 6 with FSIs off, but now more exaggerated. Achilles' low energy peak becomes much more prominent while both hA and hN remain shallow with a peak shifted slightly upward to 0.10-0.15 GeV. hA and hN agree very well with each other with hN having slightly

more low proton energy.

Adding in the momentum cut with FSIs on brings Achilles distribution closer the GENIE models (more so than when FSIs were off). This seems likely due to the effect of multi-proton events being converted into single proton events once the cut is added as seen in TAB.2.

Looking at the $n_p = 2$ distributions, we observe a convergence of the peaks to roughly 0.05-0.10 GeV (ignoring the relative event numbers). Adding in the momentum cut causes the distributions to agree even more with Achilles losing many low energy events.

Lastly, in the $n_p > 2$ distributions, we see strong similarities between Achilles and hA and somewhat hN besides its large peak. This shows us that hN's dominance in $n_p > 2$ events are all low-energy events localized to this region we observe. This is further shown when the cut is added, in which this feature is removed and models agree.

Looking at each case side by side before the cut is added, we see a trend in the distribution shapes for Achilles and hN. For Achilles, as protons are added to the final state, the distribution shape shifts upward and becomes shallower. hN appears to have the opposite trend, with its peak shifting downward and becoming more peaked. hA appears to have the same trend as hN, but does not have enough $n_p > 2$ events for it to become present.

For the 20m off-axis case, we see very similar results indicating an independence of axis position on leading kinetic energies and model relations. We add these distributions to the appendix for brevity.

We now analyze the subleading proton kinetic energies shown in FIG. 9 below.

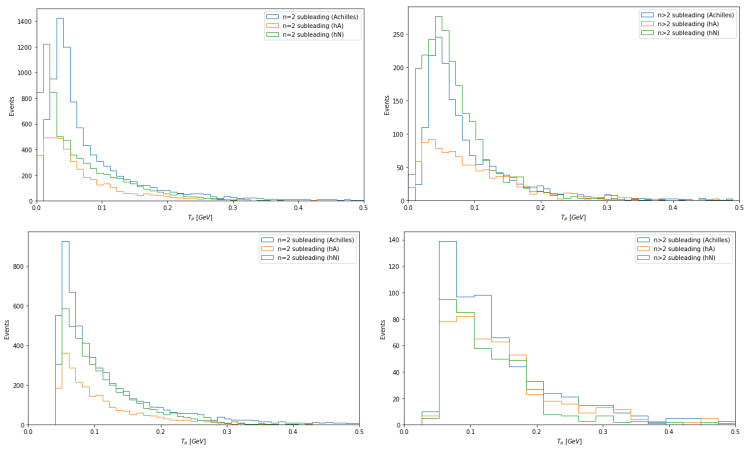

Figure 9: On-axis kinetic energies of subleading proton. Top plots are without the cut and the bottom with. The left most plots are $n_p = 2$, and right plots $n_p > 2$.

We see for both $n_p = 2$ and $n_p > 2$ cases, we see more similarities between

Achilles and GENIE than we did with the leading proton. For $n_p = 2$ we observe that hN has a similar peak to Achilles but shifted slightly lower. hA also appears to be similar but way less peak due to its lack of multi-proton events as we have discussed. When the momentum cut is added, we see the peaks converge for both multi-proton cases. For the 20m off-axis case we see very similar distributions to the on-axis cases just as we did with the leading protons and thus place them to the appendix as well.

Finally, we discuss our results for the angle between the muon and leading proton plotted below in FIG. 10 and FIG. 11 for on-axis and 20m off-axis respectively.

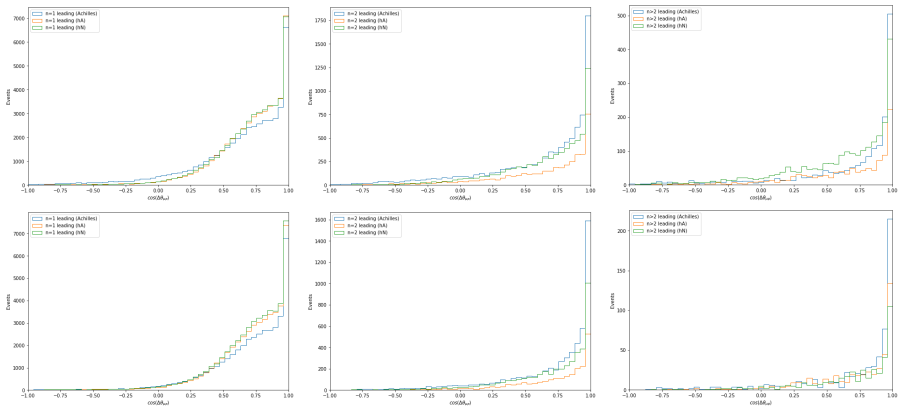

Figure 10: On-axis angle between muon and leading proton. Top plots are without the momentum cut and bottom are with. The left most plots are $n_p = 1$, middle plots $n_p = 2$, and right plots $n_p > 2$.

In the $n_p = 1$ case we see a very similar distribution to the no FSI case in FIG 7. Again, we see the same trend of the cut removing Achilles' high angle events but preserving its lack of low angle events compared to the GENIE models. For the multi-proton cases, we see better agreement between the models. The minor observed differences in hA appear to be due its lack of events in these the mult-proton categories and the differences in hN appear to be due to its dominating of $n_p > 2$ events.

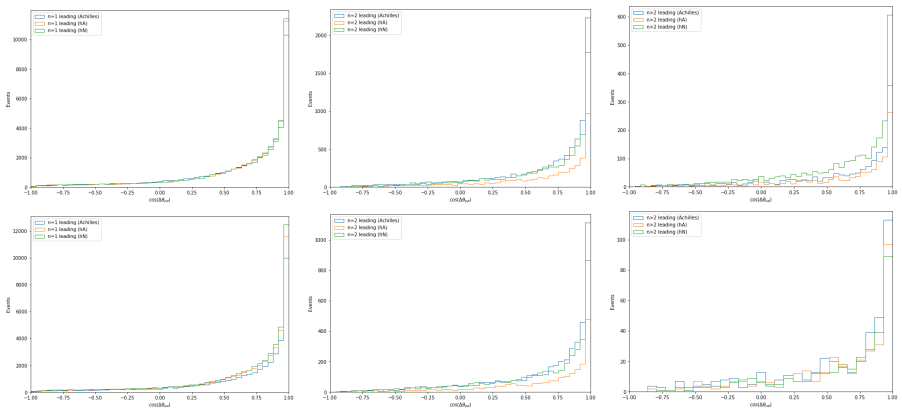

Figure 11: On-axis angle between muon and leading proton. Top plots are without the momentum cut and bottom are with. The left most plots are $n_p = 1$, middle plots $n_p = 2$, and right plots $n_p > 2$.

For the 20m off-axis case, we see the same trend as we did without FSIs in FIG.7 where models agree much better for the lower energy and more mono-energetic neutrinos supplied by the off-axis flux. Just like in the on-axis case, we see agreement in the multi-proton cases with differences being due to event numbers.

4.4 Comparisons with MicroBooNE flux

In this last section, we briefly discuss the similarities we found when using DUNE 20m off-axis flux and MicroBooNE flux to generate Achilles events. Below in FIG. 12 we display the neutrino fluxes and in FIG. 13, the kinematics we compared.

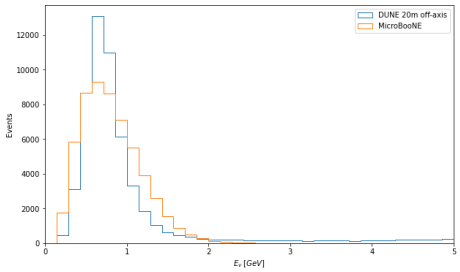

Figure 12: Neutrino spectra with DUNE 20m off-axis and MicroBooNE fluxes

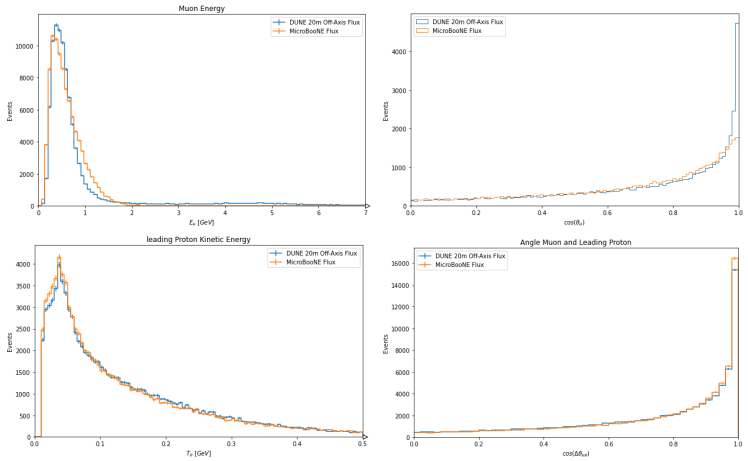

Figure 13: Top left: muon energy, top right: muon scattering angle, bottom left: leading proton energy, bottom right: angle between muon and leading proton.

In FIG. 13 we observe strong similarities in all displayed kinematics due to the similarities in the neutrino fluxes as shown in FIG. 12. However, we see a minor difference in the muon scattering angle with DUNE having more on-axis muons than MicroBooNE. This must be caused by DUNE's 20m flux being more mono-energetic compared to MicroBooNE as this is the only differing parameter in the event generation. Regardless, these strong similarities between the fluxes show that current MicroBooNE and SNB measurements will be applicable to DUNE analysis for positions around 20m.

5 Conclusions

To summarize the results of our study, we observed that Achilles and GENIE produce similarities and differences for certain kinematics due to their differing QE models, form factors, and FSIs models. We saw that differences were present even when only considering the QE models and form factors. All models agree very well on muon kinematics besides a slight difference in 20m off-axis muon scattering angles in which Achilles possesses more low angle events. For proton kinematics without FSIs, the main difference we observed was that Achilles produces more low-energy protons events compared to GENIE. For proton kinematics with FSIs, we saw this difference in $n_p = 1$ events exaggerate. For the multi-proton cases and subleading protons, we saw both similarities and differences among them.

Our results in this study motivate future studies with including more models in the comparison, repeating for different interaction channels and final state cases, and studying the differences in model choices between generators in more depth.

6 Appendix

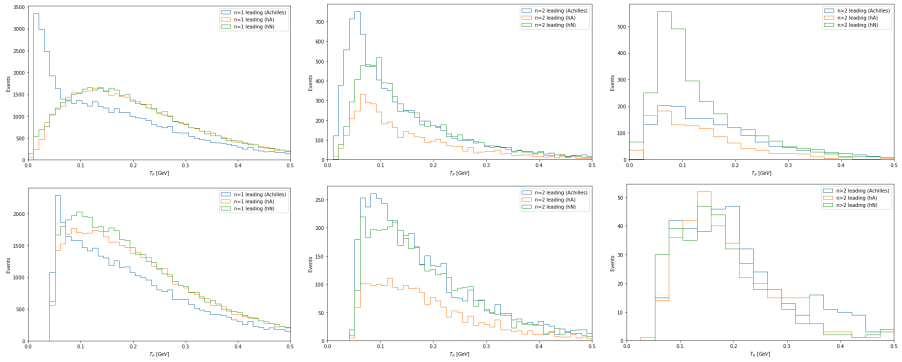

Figure 14: 20m off-axis kinetic energy of leading proton. Top plots are without the cut and the bottom with. The left most plots are $n_p = 1$, middle plots $n_p = 2$, and right plots $n_p > 2$.

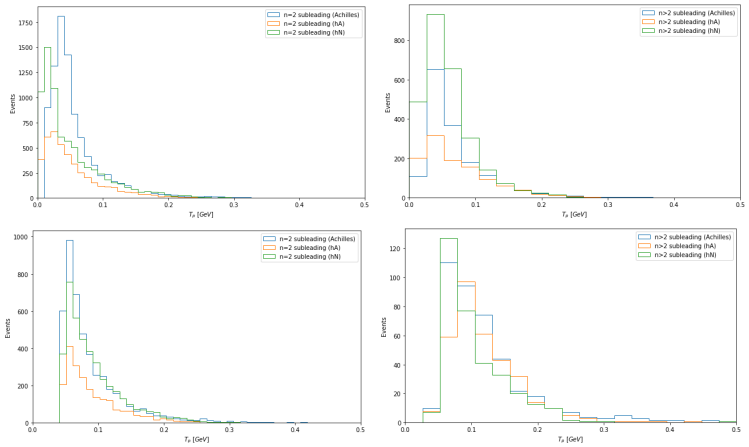

Figure 15: 20m off-axis kinetic energies of subleading proton. Top plots are without the cut and the bottom with. The left most plots are $n_p = 2$, and right plots $n_p > 2$.

This manuscript has been authored by Fermi Research Alliance, LLC under Contract No. DE-AC02-07CH11359 with the U.S. Department of Energy, Office of Science, Office of High Energy Physics. This work was supported in part by the U.S. Department of Energy, Office of Science, Office of Workforce Development for Teachers and Scientists (WDTS) under the Science Undergraduate Laboratory Internships Program (SULI).